No. 557 **January 2017**

Dynamic of Two-phase Dusty Nanofluid Flow Past a Vertical Wavy Surface

S. Siddiqa, N. Begum, M. A. Hossain

ISSN: 2190-1767

Dynamic of Two-phase Dusty Nanofluid Flow Past a Vertical Wavy Surface

Sadia Siddiqa*,[1], Naheed Begum*, M. A. Hossain§
*Department of Mathematics, COMSATS Institute of Information Technology, Kamra Road, Attock, Pakistan
§UGC Professor, Department of Mathematics, University of Dhaka, Bangladesh

1 Abstract

An analysis is performed to study two-phase natural convection flow with heat transfer of nanofluid along a vertical way surface. The model includes equations expressing conservation of total mass, momentum and thermal energy for two-phase nanofluid. Primitive variable formulations (PVF) are used to transform the dimensionless boundary layer equations into convenient coordinate system and resulting equations are integrated numerically via implicit finite difference iterative scheme. The effects of the controlling parameters on the dimensionless quantities such as skin friction coefficient, rate of heat transfer and rate of mass transfer are explored. It is concluded from present analysis, that the diffusivity ratio parameter, N_A and particle-density increment number, N_B has pronounced effect in reduction of heat transfer rate.
Keywords: Natural convection, Nanofluid, Two-phase, Dusty fluid, Wavy surface.

2 Introduction

The analysis of nanofluids have received a notable attention because of their tremendous spectrum of applications including sterilization of medical suspensions, nanomaterial processing, automotive coolants, microbial fuel cell technology, polymer coating, intelligent building design, microfluid delivery devices and aerospace tribology. The term nanofluid, first coined by Choi [1], refers to a liquid containing a dispersion of submicron solid particles (nanoparticles) having higher thermal conductivity in a base fluid. It is noteworthy that these nanoparticles are taken ultrarefine (i.e length of order 1-50nm), so that nanofluids appear to behave more like a single-phase fluid than a solid–liquid suspension. The nanoparticles used in nanofluids are usually made of chemically stable metals, oxides, carbides, nitrides, or non-metals, and the base fluid is generally a conductive fluid, such as water, ethylene glycol (or other coolants), oil (and other lubricants), polymer solutions, bio-fluids and other common fluids. Because of the enhanced heat transfer characteristics and useful applications, numerous investigations has been made on nanofluid under various physical circumstances. In this context, book by Das et al. [2] and the review papers by (see Ref. [3]-[9]) presents comprehensive discussions of the published work on convective heat transfer in nanofluids.

The investigations on flow of fluids with suspended particles have attracted the attention of numerous researchers due to their practical applications in various problem of atmospheric, engineering and physiological fields (see [10]). Farbar and Morley [11] were

[1]Corresponding Author.
Email: saadiasiddiqa@gmail.com

the first to analyze the gas-particulate suspension on experimental grounds. After that, Marble [13] studied the problem of dynamics of a gas containing small solid particles and developed the equations for gas-particle flow systems. Singleton [14] was the first to study the boundary layer analysis for dusty fluid and later on, the dynamics of two-phase flow was investigated by numerous authors (see Ref. [15]-[20]) under different physical circumstances.

It is noteworthy to mention that the irregular surfaces, say, vertical or horizontal wavy surfaces have been considered vastly in the literature (see Ref. [21]-[31]). Through these analysis, it has been reported that such surfaces serves practically in engineering applications (for instance in solar collectors, grain storage containers, industrial heat exchangers and condensers in refrigerators). Motivated by the previous works and possible applications, natural convection flow of two-phase dusty nanofluid is modeled along a vertical wavy surface in the present study. The nanoparticles are assumed to move due to such phenomena as Brownian motion and thermophoresis and are carried by the flow of the base fluid. Furthermore, water is taken as continuous base fluid that contains dust particles in it. Taking Grashof number Gr to be very large, the boundary layer approximation is invoked leading to a set of non-similar parabolic partial differential equations whose solution is obtained through implicit finite difference method. From the present analysis we will interrogate whether the presence of dust particles in nanofluid affects the physical characteristics associates with the wavy surfaces or not? The computational data is presented graphically in the form of wall shear stress, heat transfer rate, mass transfer rate, streamlines and isotherms by varying several controlling parameters.

3 Flow Analysis

A two-dimensional natural convection flow of two-phase dusty nanofluid is modeled along a vertical wavy surface. The boundary layer analysis outlined below allows the shape of the wavy surface, $\bar{y}_w = \bar{\sigma}(\bar{x})$, to be arbitrary, but our detailed numerical work will assume that the surface exhibits sinusoidal deformations. Therefore, the shape of the wavy surface profile is assumed to pursue the following pattern:

$$\bar{y}_w = \bar{\sigma}(\bar{x}) = \bar{a}\sin\left(\frac{2\pi\bar{x}}{L}\right) \tag{1}$$

where $\bar{a}$ is the amplitude of the transverse surface wave and L is the characteristic length associated with the wave. Overbars denote dimensional quantities.The surface of vertical wavy plate is maintained at a constant temperature T_w, which is higher than the ambient temperature T_∞. The physical model and coordinate system are shown in Fig 1. The assumption of two-phase flow has been extensively analyzed in the past (for details see Ref. [12], [20]), and the equations describing the complete description of the convective flow along the vertical surface can be written in dimensional form as:
For gas phase:

$$\frac{\partial\bar{u}}{\partial\bar{x}} + \frac{\partial\bar{v}}{\partial\bar{y}} = 0 \tag{2}$$

$$\rho_f\left(\bar{u}\frac{\partial\bar{u}}{\partial\bar{x}} + \bar{v}\frac{\partial\bar{u}}{\partial\bar{y}}\right) = -\frac{\partial\bar{p}}{\partial\bar{x}} + \mu_f\nabla^2\bar{u} + \rho_f g\beta(T-T_\infty)(1-\phi_\infty) - g(\rho_p-\rho_g)(\phi-\phi_\infty) + \frac{\rho_p}{\tau_m}(\bar{u}_p-\bar{u}) \tag{3}$$

$$\rho_f \left(\bar{u}\frac{\partial \bar{v}}{\partial \bar{x}} + \bar{v}\frac{\partial \bar{v}}{\partial \bar{y}} \right) = -\frac{\partial \bar{p}}{\partial \bar{y}} + \mu_f \nabla^2 \bar{v} + \frac{\rho_p}{\tau_m}(\bar{v}_p - \bar{v}) \tag{4}$$

$$\begin{aligned}\rho_f c_f \left(\bar{u}\frac{\partial T}{\partial \bar{x}} + \bar{v}\frac{\partial T}{\partial \bar{y}} \right) = \kappa_f \nabla^2 T + (\rho c)_{np} \left(D_B \nabla\phi.\nabla T + \frac{D_T}{T_\infty}\nabla T.\nabla T \right) + \frac{\rho_p c_s}{\tau_T}(T_p - T) \\ + \frac{\rho_p}{\tau_m}\{(\bar{u}_p - \bar{u})^2 + (\bar{v}_p - \bar{v})^2\}\end{aligned} \tag{5}$$

$$\bar{u}\frac{\partial \phi}{\partial \bar{x}} + \bar{v}\frac{\partial \phi}{\partial \bar{y}} = D_B \nabla^2 \phi + \frac{D_T}{T_\infty}\nabla^2 T \tag{6}$$

For the particle phase:

$$\frac{\partial \bar{u}_p}{\partial \bar{x}} + \frac{\partial \bar{v}_p}{\partial \bar{y}} = 0 \tag{7}$$

$$\rho_p \left(\bar{u}_p\frac{\partial \bar{u}_p}{\partial \bar{x}} + \bar{v}_p\frac{\partial \bar{u}_p}{\partial \bar{y}} \right) = -\frac{\partial \bar{p}_p}{\partial \bar{x}} - \frac{\rho_p}{\tau_m}(\bar{u}_p - \bar{u}) \tag{8}$$

$$\rho_p \left(\bar{u}_p\frac{\partial \bar{v}_p}{\partial \bar{x}} + \bar{v}_p\frac{\partial \bar{v}_p}{\partial \bar{y}} \right) = -\frac{\partial \bar{p}_p}{\partial \bar{y}} - \frac{\rho_p}{\tau_m}(\bar{v}_p - \bar{v}) \tag{9}$$

$$\rho_p c_s \left(\bar{u}_p\frac{\partial T_p}{\partial \bar{x}} + \bar{v}_p\frac{\partial T_p}{\partial \bar{y}} \right) = -\frac{\rho_p c_s}{\tau_T}(T_p - T) \tag{10}$$

where $(\bar{u}, \bar{v})$, T, ϕ, $\bar{p}$, ρ_f, c_f, β κ_f, μ_f are respectively the velocity vector in the $(\bar{x}, \bar{y})$ direction, temperature, concentration of nanoparticles, pressure, density, specific heat at constant pressure, volumetric expansion coefficient, thermal conductivity and kinematic viscosity of the suspension of nanofluid. Similarly, $(\bar{u}_p, \bar{v}_p)$, T_p, $\bar{p}_p$, ρ_p and c_s corresponds to the velocity vector, temperature, pressure, density and specific heat for the particle phase. In addition, g the gravitational acceleration, τ_m (τ_T) the momentum relaxation time (thermal relaxation time) for dust particles, ϕ_w the nanoparticle volume fraction near the surface, ϕ_∞ the nanoparticle volume fraction at outer edge of boundary layer region, ρ_{np} the density of the nanoparticles, D_B the Brownian diffusion coefficient and D_T the thermophoretic diffusion coefficient.

The fundamental equations stated above are to be solved under appropriate boundary conditions to determine the flow fields of the fluid and the dust particles. Therefore, the boundary conditions for the problem under considerations are: For gas phase:

$$\begin{aligned}\bar{u}(\bar{x}, \bar{y}_w) = \bar{v}(\bar{x}, \bar{y}_w) = T(\bar{x}, \bar{y}_w) - T_w = \phi(\bar{x}, \bar{y}_w) - \phi_w = 0 \\ \bar{u}(\bar{x}, \infty) = T(\bar{x}, \infty) - T_\infty = \phi(\bar{x}, \infty) = 0\end{aligned} \tag{11}$$

For particle phase:

$$\begin{aligned}\bar{u}_p(\bar{x}, \bar{y}_w) = \bar{v}_p(\bar{x}, \bar{y}_w) = T_p(\bar{x}, \bar{y}_w) - T_w = 0 \\ \bar{u}_p(\bar{x}, \infty) = T_p(\bar{x}, \infty) - T_\infty = 0\end{aligned} \tag{12}$$

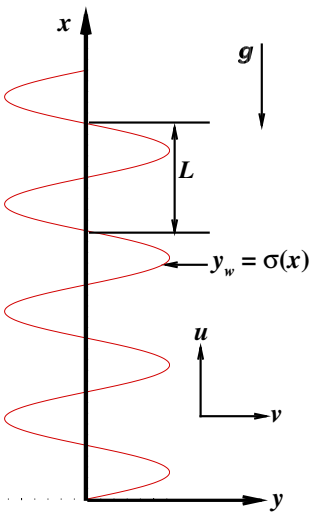

Fig. 1 Physical Model

In order to transform all the above-mentioned quantities in Eqs. (2)-(12) in uniform order of magnitude, the following continuous dimensionless variables have been employed:

$$x=\frac{\bar{x}}{L},\quad y=\frac{\bar{y}-\bar{\sigma}(\bar{x})}{L}Gr_L^{1/4},\quad (\bar{u},\bar{u}_p)=\frac{\nu_f Gr_L^{1/2}}{L}(u,u_p),\quad (\bar{v},\bar{v}_p)-\sigma_x(\bar{u},\bar{u}_p)=\frac{\nu_f Gr_L^{1/4}}{L}(v,v_p),$$
$$a=\frac{\bar{a}}{L},\quad (\bar{p},\bar{p}_p)=\frac{Gr_L\rho_f\nu_f^2}{L^2}(p,p_p),\quad (\theta,\theta_p)=\frac{(T,T_p)-T_\infty}{T_w-T_\infty},\quad C=\frac{\phi-\phi_\infty}{\phi_w-\phi_\infty},\quad \sigma=\frac{\bar{\sigma}}{L},$$
$$\sigma_x=\frac{d\bar{\sigma}}{d\bar{x}}=\frac{d\sigma}{dx},\quad Gr_L=\frac{g\beta(1-\phi_\infty)(T_w-T_\infty)L^3}{\nu_f^2},\quad Nr=\frac{(\rho_p-\rho_f)(\phi_w-\phi_\infty)}{\rho_f\beta(1-\phi_\infty)(T_w-T_\infty)},$$
$$\mathrm{Pr}=\frac{\nu_f}{\alpha},\quad N_A=\frac{D_T(T_w-T_\infty)}{D_BT_\infty(\phi_w-\phi_\infty)},\quad N_B=\tau(\phi_w-\phi_\infty),\quad Ln=\frac{\nu_f}{D_B},\quad Ec=\frac{\nu_f^2Gr_L}{(T_w-T_\infty)c_p} \tag{13}$$

By incorporating Eq. (13), the dimensional continuity, momentum and temperature equations for both phases will be transformed in underlying form.
For the gas phase:

$$\frac{\partial u}{\partial x}+\frac{\partial v}{\partial y}=0 \tag{14}$$

$$u\frac{\partial u}{\partial x}+v\frac{\partial u}{\partial y}=-\left(\frac{\partial p}{\partial x}-\sigma_xGr_L^{1/4}\frac{\partial p}{\partial y}\right)+\left(1+\sigma_x^2\right)\frac{\partial^2u}{\partial y^2}+\theta-NrC+D_\rho\alpha_d(u_p-u) \tag{15}$$

$$\sigma_x\left(u\frac{\partial u}{\partial x}+v\frac{\partial u}{\partial y}\right)+u^2\sigma_{xx}=-Gr_L^{1/4}\frac{\partial p}{\partial y}+\sigma_x\left(1+\sigma_x^2\right)\frac{\partial^2u}{\partial y^2}+D_\rho\alpha_d\sigma_x(u_p-u) \tag{16}$$

$$u\frac{\partial\theta}{\partial x}+v\frac{\partial\theta}{\partial y}=\left(1+\sigma_x^2\right)\left[\frac{1}{\mathrm{Pr}}\frac{\partial^2\theta}{\partial y^2}+\frac{N_B}{Ln}\left(\frac{\partial C}{\partial y}\right)\left(\frac{\partial\theta}{\partial y}\right)+\frac{N_AN_B}{Ln}\left(\frac{\partial\theta}{\partial y}\right)^2\right]+\frac{2}{3\mathrm{Pr}}D_\rho\alpha_d(\theta_p-\theta)$$
$$+D_\rho\alpha_dEc\left(1+\sigma_x^2\right)(u_p-u)^2 \tag{17}$$

$$u\frac{\partial C}{\partial x}+v\frac{\partial C}{\partial y}=\frac{\left(1+\sigma_x^2\right)}{Ln}\left(\frac{\partial^2 C}{\partial y^2}+N_A\frac{\partial^2\theta}{\partial y^2}\right) \tag{18}$$

For particle phase:

$$\frac{\partial u_p}{\partial x}+\frac{\partial v_p}{\partial y}=0 \tag{19}$$

$$u_p\frac{\partial u_p}{\partial x}+v_p\frac{\partial u_p}{\partial y}=-\frac{\partial p_p}{\partial x}+\sigma_x Gr^{1/4}\frac{\partial p_p}{\partial y}-\alpha_d(u_p-u) \tag{20}$$

$$\sigma_x\left(u_p\frac{\partial u_p}{\partial x}+v_p\frac{\partial u_p}{\partial y}\right)+u_p^2\sigma_{xx}=-Gr^{1/4}\frac{\partial p_p}{\partial y}-\alpha_d\sigma_x(u_p-u) \tag{21}$$

$$u_p\frac{\partial \theta_p}{\partial x}+v_p\frac{\partial \theta_p}{\partial y}=-\frac{2}{3\gamma\mathrm{Pr}}\alpha_d(\theta_p-\theta) \tag{22}$$

In the above system of equations, (u, v) are (x, y) components of the velocity field, p the pressure, θ the dimensionless temperature and C the nanoparticle concentration in boundary layer region. In the above expressions, Gr_L, Pr, Ec, Nr and Ln are respectively the Grashof number, Prandtl number, Eckrect number, buoyancy ratio parameter and nanoparticle Lewis number. Furthermore, modified diffusivity ratio and particle-density increment are respectively denoted by N_A and N_B and $\tau=(\rho c)_{np}/(\rho c)_f$ the ratio of heat capacity of nanofluid to the heat capacity of the base fluid. The dimensionless mathematical expressions for the interaction of two-phases are gives as:

$$\gamma=\frac{c_s}{c_f},\quad \tau_T=\frac{3}{2}\gamma\tau_m\mathrm{Pr},\quad D_\rho=\frac{\rho_p}{\rho_f},\quad \alpha_d=\frac{L^2}{\tau_m\nu_f Gr_L^{1/2}} \tag{23}$$

where, γ, D_ρ, α_d are respectively symbolizing the specific heat ratio of the mixture, mass concentration of particle phase and the dust parameter. It is important to mention here that for different mixtures, the interaction term γ may vary between 0.1 and 10.0 (For details see [10]). It can also be observed that for $\alpha_d=0.0$, the flow governs by the natural convection in the absence of the dusty particles (i.e carrier phase only). It should be noted that Eqs. (15) and (20) indicates the pressure gradient along y direction is of $O(Gr_L^{-1/4})$, which implies that the lower order of pressure gradient along x direction can be determined from the inviscid flow solution. However, this pressure gradient is zero, since there is no externally induced free stream. It can be further noted from Eqs. (15) and (20) that the terms $Gr_L^{1/4}\partial p/\partial y$ and $Gr_L^{1/4}\partial p_p/\partial y$ are of $O(1)$ and can be determined by the left-hand side of these equations. By solving the Eqs. (15)-(16) and (20)-(21) simultaneously, the resulting equations for carrier as well as particle phase can be in the form of:

$$u\frac{\partial u}{\partial x}+v\frac{\partial u}{\partial y}+\frac{\sigma_x\sigma_{xx}}{(1+\sigma_x^2)}u^2=\left(1+\sigma_x^2\right)\frac{\partial^2 u}{\partial y^2}+\frac{(\theta-NrC)}{(1+\sigma_x^2)}+D_\rho\alpha_d(u_p-u) \tag{24}$$

$$u_p\frac{\partial u_p}{\partial x}+v_p\frac{\partial u_p}{\partial y}+\frac{\sigma_x\sigma_{xx}}{(1+\sigma_x^2)}u_p^2=-D_\rho\alpha_d(u_p-u) \tag{25}$$

The dimensionless form of the boundary conditions for present analysis are of the underlying form.

For gas phase:

$$\begin{gathered}u(x,0)=v(x,0)=\theta(x,0)-1=C(x,0)-1=0\\ u(x,\infty)=\theta(x,\infty)=C(x,\infty)=0\end{gathered} \tag{26}$$

For particle phase:

$$\begin{gathered} u_p(x,0) = v_p(x,0) = \theta_p(x,0) - 1 = 0 \\ u_p(x,\infty) = \theta_p(x,\infty) = 0 \end{gathered} \tag{27}$$

For numerical treatment for the present problem, we have employed the implicit finite difference (Thomas Algorithm). For this, first we introduce the following transformations to reduce the system of boundary layer equations into some convenient form:

$$x = X, \quad y = Y x^{\frac{1}{4}}, \quad (u, u_p) = x^{\frac{1}{2}}(U, U_p), \quad (v, v_p) = x^{\frac{-1}{4}}(V, V_p), \quad (\theta, \theta_p) = (\Theta, \Theta_p), \quad C = C \tag{28}$$

By incorporating the transformation defined in Eq. (28), the above system of dimensionless boundary layer equations can be further mapped into the non-conserved form as follows:
For gas phase:

$$\frac{1}{2}U + X\frac{\partial U}{\partial X} - \frac{Y}{4}\frac{\partial U}{\partial Y} + \frac{\partial V}{\partial Y} = 0 \tag{29}$$

$$\left(\frac{1}{2} + \frac{X\sigma_X\sigma_{XX}}{\left(1+\sigma_X^2\right)}\right)U^2 + XU\frac{\partial U}{\partial X} + \left(V - \frac{YU}{4}\right)\frac{\partial U}{\partial Y} = \left(1+\sigma_X^2\right)\frac{\partial^2 U}{\partial Y^2} + \frac{(\Theta - NrC)}{\left(1+\sigma_X^2\right)} + D_\rho\alpha_d X^{1/2}(U_p - U) \tag{30}$$

$$XU\frac{\partial \Theta}{\partial X} + \left(V - \frac{YU}{4}\right)\frac{\partial \Theta}{\partial Y} = (1+\sigma_X^2)\left[\frac{1}{\mathrm{Pr}}\frac{\partial^2\Theta}{\partial Y^2} + \frac{N_B}{Ln}\left(\frac{\partial C}{\partial Y}\right)\left(\frac{\partial \Theta}{\partial Y}\right) + \frac{N_A N_B}{Ln}\left(\frac{\partial \Theta}{\partial Y}\right)^2\right] + D_\rho\alpha_d\left((1+\sigma_X^2)EcX^{3/2}(U_p - U)^2 + \frac{2}{3\mathrm{Pr}}X^{1/2}(\Theta_p - \Theta)\right) \tag{31}$$

$$XU\frac{\partial C}{\partial X} + \left(V - \frac{YU}{4}\right)\frac{\partial C}{\partial Y} = \frac{\left(1+\sigma_X^2\right)}{Ln}\left(\frac{\partial^2 C}{\partial Y^2} + N_A\frac{\partial^2\Theta}{\partial Y^2}\right) \tag{32}$$

For particle phase:

$$\frac{1}{2}U_p + X\frac{\partial U_p}{\partial X} - \frac{1}{4}Y\frac{\partial U_p}{\partial Y} + \frac{\partial V_p}{\partial Y} = 0 \tag{33}$$

$$\left(\frac{1}{2} + \frac{X\sigma_X\sigma_{XX}}{\left(1+\sigma_X^2\right)}\right)U_p^2 + XU_p\frac{\partial U_p}{\partial X} + \left(V_p - \frac{1}{4}YU_p\right)\frac{\partial U_p}{\partial Y} = -\alpha_d X^{1/2}(U_p - U) \tag{34}$$

$$XU_p\frac{\partial \Theta_p}{\partial X} + \left(V_p - \frac{1}{4}YU_p\right)\frac{\partial \Theta_p}{\partial Y} = -\frac{2}{3\gamma\mathrm{Pr}}\alpha_d X^{1/2}\left(\Theta_p - \Theta\right) \tag{35}$$

The transformed boundary conditions can be written as:

$$\begin{gathered} U(X,0) = V(X,0) = \Theta(X,0) - 1 = C(X,0) - 1 = U_p(X,0) = V_p(X,0) = \Theta_p(X,0) - 1 = 0 \\ U(X,\infty) = U_p(X,\infty) = \Theta(X,0) = \Theta_p(X,\infty) = C(X,\infty) = 0 \end{gathered} \tag{36}$$

4 Solution Methodology

The nonlinear interaction among the continuity, momentum and energy equations of carrier and disperse phase, given in (29) to (35) subject to the boundary conditions (37), are solved

numerically with the aid of the implicit finite difference method which implies Thomas algorithm as a solver. Since the equations are parabolic in X therefore solutions can be marched in the downstream direction. The computational domain is discretized over the entire boundary layer region. Keeping numerical stability in view, two-point central difference and backward difference quotients are respectively used for diffusion and convective terms. The resulting system of algebraic equations can be cast into a tri-diagonal matrix equation which is solved via Thomas algorithm. This algorithm works on the following pattern:

1. Set the suitable initial and boundary conditions.
2. Solve the unknowns $U, U_p, C, \Theta, \Theta_p$ at $Y = 0$. It means that these unknowns satisfy the convergence criteria.
3. Solve for the next step $Y_j = Y_{j-1} + \Delta Y$ by using the solution position.
4. The computations are iterated until the unknown quantities meet the convergence criteria at the streamwise position. The convergence criteria is:

$$(max|U_{i,j}| + max|U_p i,j| + max|V_{i,j}| + max|V_p i,j| + max|\Theta_{i,j}| + max|\Theta_p i,j| + max|C_{i,j}|) \leq 10^{-6} \quad (37)$$

5. Repeat step 2-4 for X maximum.

In the computation procedure, continuity equation of the carrier and the particle phase are used to obtain normal velocity component V and V_p respectively by using the following discretization:

$$V_{i,j} = V_{i-1,j} + \frac{1}{4}Y\left(U_{i,j} - U_{i-1,j}\right) - \frac{1}{2}\triangle Y U_{i,j} - \frac{1}{2}\frac{X\triangle Y}{\triangle X}\left(U_{i,j} - U_{i,j-1} + U_{i-1,j} - U_{i-1,j-1}\right) \quad (38)$$

$$V_{p_{i,j}} = V_{p_{i-1,j}} + \frac{1}{4}Y\left(U_{p_{i,j}} - U_{p_{i-1,j}}\right) - \frac{1}{2}\triangle Y U_{p_{i,j}} - \frac{1}{2}\frac{X\triangle Y}{\triangle X}\left(U_{p_{i,j}} - U_{p_{i,j-1}} + U_{p_{i-1,j}} - U_{p_{i-1,j-1}}\right) \quad (39)$$

At present, rectangular computational domain is used with grid point distribution at equal spacing. Additionally, 1501 uniform grid points are employed in normal Y direction as well as in marching X direction. In the program test, a finer axial step size, $\triangle X = X_i - X_{i-1} = 0.006$, is found to give acceptable accuracy. The computation has been started from $X_i = 0.01$ and then marched up to $X_i = 10.0$ by taking uniform grids. By comparing the results for different grid size in Y directions, we reached at the conclusion to choose $\triangle Y = Y_j - Y_{j-1} = 0.02$ and the value of the boundary layer Y_∞ is 35.0 which actually corresponds to the condition $Y \to \infty$ and it lies very well outside the momentum and thermal boundary layers of the corresponding phase. Implicit finite difference scheme is unconditionally stable and compatible and hence ensures convergence.

As the knowledge of drag force in terms of skin friction is a prime factor to apprehend the behavior of any fluid/gas machinery system or component. Therefore, the physical quantity, namely, skin friction, is of significant importance both scientifically and experimentally. In addition to skin friction, it is also important to investigate the behavior of the

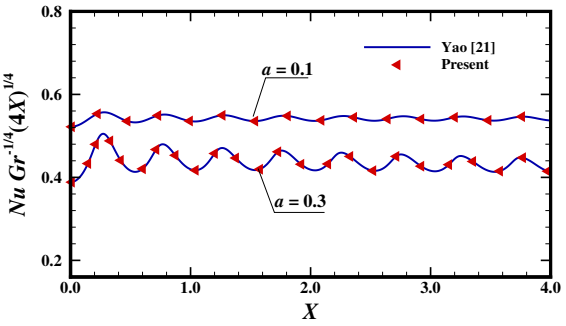

Fig. 2 Local Nusselt number coefficient for $a = 0.1, 0.3$**, while** $D_\rho = 0.0$**,** $\mathbf{Pr} = 1.0$**,** $\alpha_d = 0.0$**,** $Nr = 0.0$**,** $N_A = N_B = 0.0$ **and** $\gamma = 1.0$**.**

heat as well as mass transfer rate, in terms of Nusselt number coefficient and Sherwood number coefficient, respectively. These quantities are much significant from engineering point of view, as rate of heat transfer can be served to improve specifically the efficiency and shape of many equipments in aerodynamics. The values of these dimensionless coefficients can be calculated from the following mathematical relations:

$$\begin{aligned} \tau_w &= C_f \left(Gr_L/X\right)^{-1/4} = \left(1+\sigma_X^2\right)^{1/2} \left(\frac{\partial U}{\partial Y}\right)_{Y=0} \\ Q_w &= Nu \left(Gr_L/X\right)^{-1/4} = -\left(1+\sigma_X^2\right)^{1/2} \left(\frac{\partial \Theta}{\partial Y}\right)_{Y=0} \\ M_w &= Sh \left(Gr_L/X\right)^{-1/4} = -\left(1+\sigma_X^2\right)^{1/2} \left(\frac{\partial C}{\partial Y}\right)_{Y=0} \end{aligned} \tag{40}$$

5 Results and Discussions

The main purpose of present analysis is to understand the behavior of two-phase dusty nanofluid along a vertical wavy surface. We performed two-dimensional simulations in order to obtain solutions of mathematical model presented in terms of primitive variables given in Eqs. (29)-(37) from the two-point implicit finite difference method. Numerical results are reported for the overall effectiveness of mass concentration of dust particles and nanoparticles in base fluid (water) moving along a transverse geometry. Particularly, the solutions are established for the water-based dusty nanofluid (i.e, $\mathrm{Pr} = 7.0$, $D_\rho = 10.0$ and $\gamma = 0.1$). The parametric values for water particulate suspension are taken from study of Apazidis [32]. While the numerical computations are performed by setting the values of other parameters as: $Nr = (0.0, 0.1)$, $N_A = (0.0, 5.0, 10.0)$, $N_B = (0.0, 5.0, 10.0, 20.0)$, $Ln = 100.0$, $\alpha_d = 0.01$, $Ec = (0.0, 0.5, 1.0)$ and $a = (0.3, 0.5, 0.8)$. For verification, simulated results are compared with the published results and it is found that the solutions obtained by Yao [21] can be recovered by setting $a = 0.1, 0.3$, $\mathrm{Pr} = 1.0$, $\alpha_d = 0.0$ $N_A = N_B = Nr = 0.0$ and $D_\rho = 0.0$. This comparison is appeared in Fig. 2 and results matches well with each other and shows good accuracy.

The influence of buoyancy ratio parameter, Nr, on skin friction coefficient, τ_w, heat transfer coefficient, Q_w and mass transfer coefficient, M_w is illustrated in Fig. 3. For com-

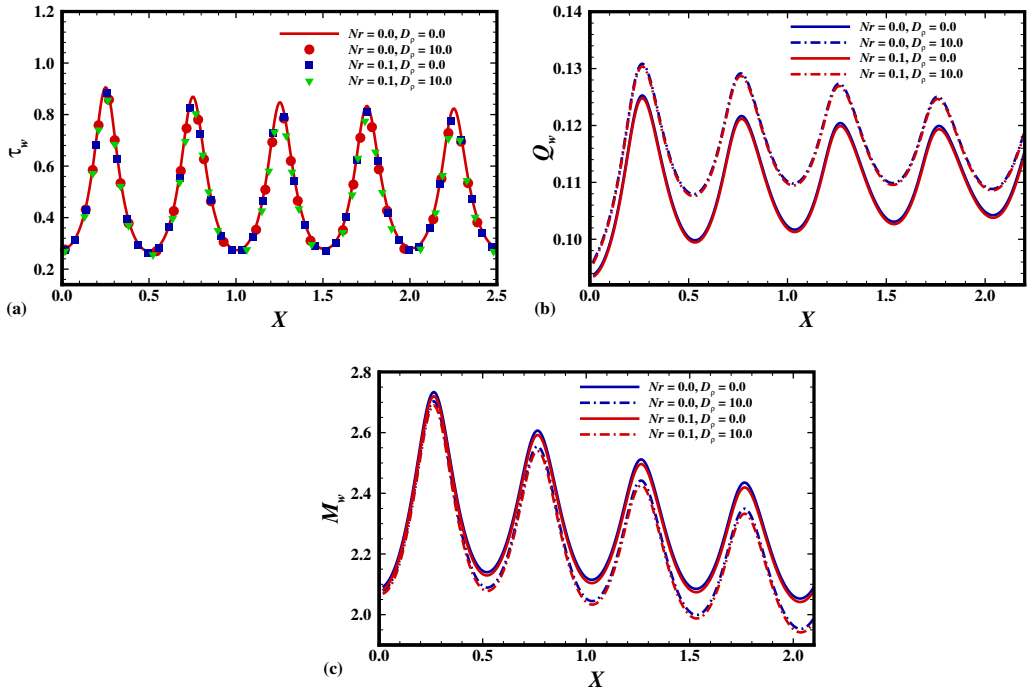

Fig. 3(a) τ_w**, (b)** Q_w **and (c)** M_w **for** $Nr = (0.0, 0.1)$**,** $D_\rho = (0.0, 10.0)$ **while Pr** $= 7.0$**,** $\gamma = 0.1$**,** $\alpha_d = 0.01$**,** $Ec = 1.0$**,** $N_A = 5.0$**,** $N_B = 10.0$**,** $Ln = 100.0$ **and** $a = 0.3$**.**

parison, the effect of Nr on water-based nanofluid without dust particles (i.e, $D_\rho = 0.0$) is also presented. It is also important to mention here that the parameter Nr is responsible for the coupling between the dimensionless nanoparticle concentration and momentum equation (See Eqn. (30)). As it can be visualize from Fig. 3(a) skin friction coefficient for dusty as well as clear fluid remains almost invariant under the variations of parameter Nr. However, variations are recorded for rate of heat transfer as well as for mass transfer coefficient by magnifying the value of buoyancy parameter, Nr (see Figs. 3(b) and 3(b)). The effect of, Nr, on average, is to reduce the Q_w and M_w for clear as well as dusty fluid. But the plots in Fig. 3(b) reveals the fact that the rate of heat transfer is extensively promoted by loading the dust particles into the base fluid (i.e, $D_\rho = 10.0$). Such behavior is expected because the base fluid gains the thermal energy from the dust particles collision which ultimately promote the rate of heat transfer near the vicinity of wavy plate. Higher the value of D_ρ, the greater will be the rate of heat transfer. On the other hand, D_ρ has a retarding influence on rate of mass transfer, which is sufficiently reduced when D_ρ is penetrated into the mechanism. As expected, higher concentration of dust particles causes the mass transfer rate to reduce near the axis of flow.

The results for water-based nanoparticulate suspension are represented in terms of τ_w, Q_w and M_w in Fig. 4. In this figure mass concentration parameter D_ρ characterizes the influence of particles on their surroundings together with the effect of Eckrect number Ec. The skin friction coefficient, τ_w remains uniform for overall range D_ρ and Ec (see Fig. 4(a)). However, a large enhancement in the heat transfer rate (Q_w) and little reduction in

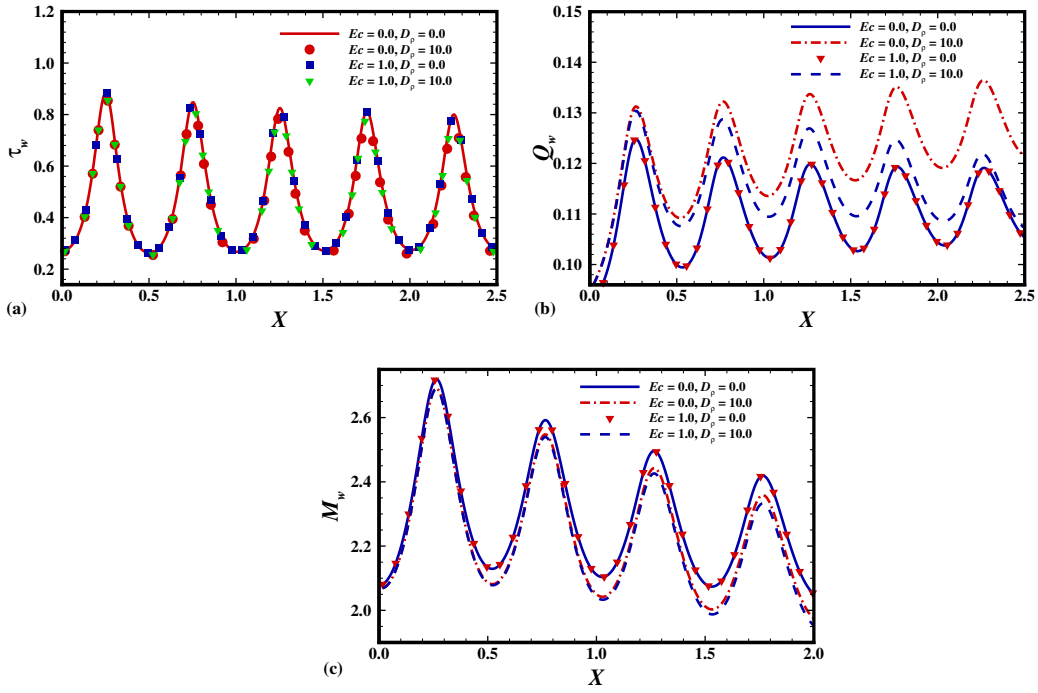

Fig. 4(a) τ_w**, (b)** Q_w **and (c)** M_w **for** $Ec = (0.0, 1.0)$**,** $D_\rho = (0.0, 10.0)$ **while Pr** $= 7.0$**,** $\gamma = 0.1$**,** $\alpha_d = 0.01$**,** $Nr = 0.1$**,** $N_A = 5.0$**,** $N_B = 10.0$**,** $Ln = 100.0$ **and** $a = 0.3$**.**

the rate of mass transfer coefficient (M_w) is recorded when mass concentration parameter and Eckrect number increases (see Figs. 4(b) and 4(c)). As it is already mentioned that, for the heat transfer rate, the dusty water gains some thermal energy from particles and consequently the temperature gradient for the carrier fluid increases. By loading the dust particles together with higher values of Ec, causes the carrier fluid to be more condense which leads to decrease the rate of mass transfer in stream-wise direction. Moreover, it is intersecting to note that, the non-zero values of Ec only increase (decrease) the rate of heat transfer (rate of mass transfer) for non-zero values of D_ρ. It can be concluded from the present study that the Eckrect number Ec has a dominating influence on water particulate suspension as compared to clear fluid.

Fig. 5 is plotted to visualize the effect of amplitude of wavy surface on the distribution of physical quantities, namely, τ_w, Q_w and M_w. The change in surface contour is followed by raise and fall of the curves. As it can be visualize from Fig. 5(a), that the influence of amplitude a, on average, is to reduce the rate of skin friction. Similar behavior is recorded for the rate of heat transfer (see Fig. 5(b)). As a whole, the rate of heat transfer, Q_w, reduces when the amplitude of the sinusoidal waveform increases. As the amplitude increases the shape of the wave gradually changes from sinusoidal waveform to the unusual shape. The reduction in the magnitude of the temperature gradient happened due to the simultaneous influence of centrifugal and buoyancy force. Furthermore, we notice that the change in rate of heat transfer is more pronounced for larger values of the amplitude a and this factor acts as a retarding force for heat transfer coefficient. As expected, the surface

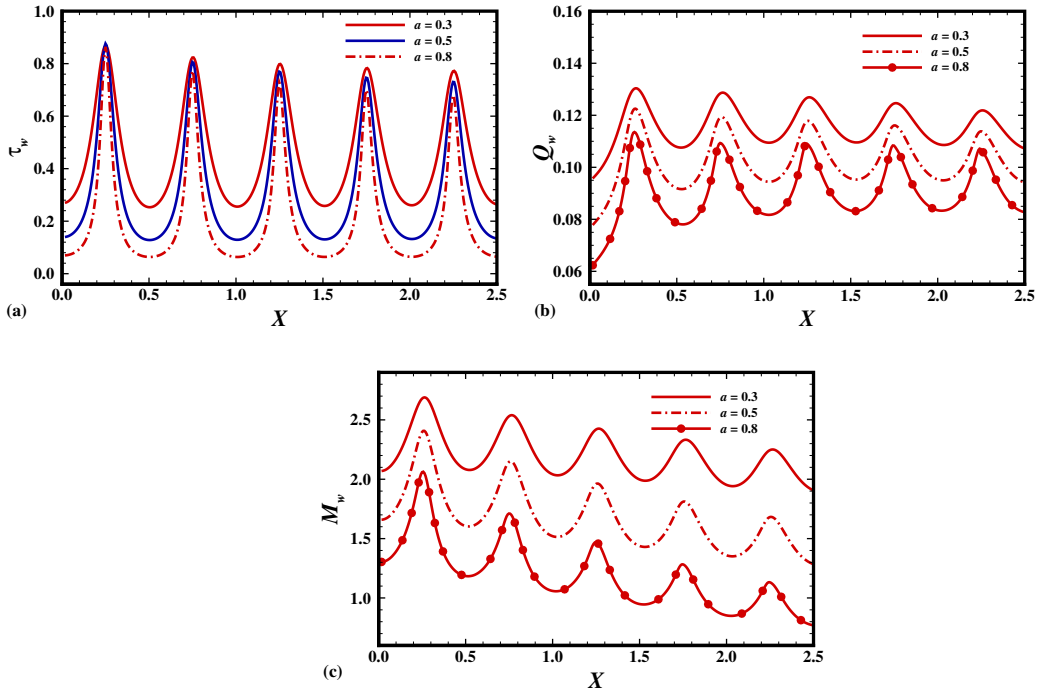

Fig. 5(a) τ_w**, (b)** Q_w **and (c)** M_w **for** $a = (0.3, 0.5, 0.8)$ **while** $D_\rho = 10.0$ **Pr** $= 7.0$**,** $\gamma = 0.1$**,** $\alpha_d = 0.01$**,** $Ec = 1.0$**,** $Nr = 0.1$**,** $N_A = 5.0$**,** $N_B = 10.0$ **and** $Ln = 100.0$**.**

having large amplitude causes a reduction in rate of mass transfer (see Fig. 5(b)). As it can be seen from Fig. 5(b), that M_w is maximum for small values of a and depicts a clear decline by increasing the amplitude of wavy surface from 0.3 to 0.8. This may happen because of the fact that the geometry having a transverse nature offers more resistance to water particulate suspension and ultimately the rate of mass transfer sufficiently decreases.

Fig. 6. anticipates the influence of modified diffusivity ratio parameter, N_A, on the distribution of skin friction coefficient, rate of heat transfer and rate of mass transfer coefficient. The variation of N_A is shown against the stream-wise coordinate X. The graph in Fig. 6(b) shows a clear decline in value of heat transfer coefficient. It is interesting to note that N_A not only reduce the rate of heat transfer but also affect the amplitude of the curves representing Q_w. The rate of heat transfer is maximum for $N_A = 0.0$ and reduced drastically for non-zero values of modified diffusivity ratio parameter. This concludes that modified diffusivity ratio parameter offer great resistance to the motion of the fluid. Therefore N_A is much more influential in the boundary layer region. This is expected because the viscous diffusion rate increases due to an increase in N_A which results in significant reduction in Q_w. But on the other hand, skin friction coefficient and mass transfer coefficient are enhanced for higher values of N_A as depicted in Figs. 6(a) and 6(c). Specifically, Fig. 6(c) ensures that the effect of N_A on mass transfer coefficient is more pronounced for higher values of N_A.

The influence of particle-density increment number, N_B, is observed in Fig. 7. The figure depicts an interesting behavior of N_B on (a) τ_w, (b) Q_w and (c) M_w. It is evident from

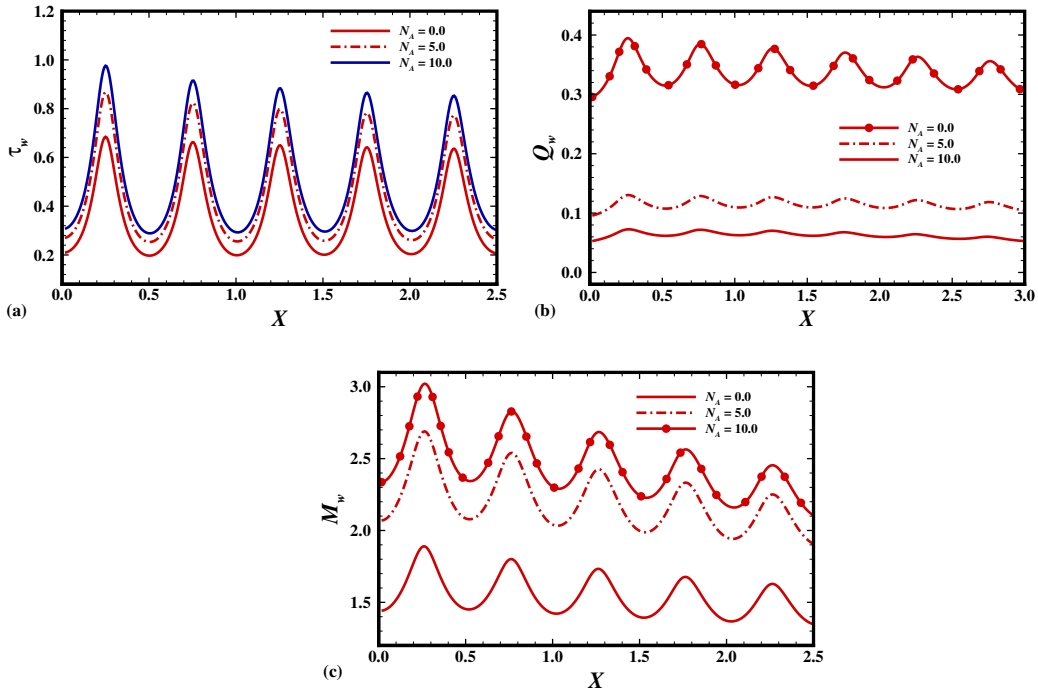

Fig. 6(a) τ_w**, (b)** Q_w **and (c)** M_w **for** $N_A = (0.0, 5.0, 10.0)$ **while** $D_\rho = 10.0$ **Pr** $= 7.0$**,** $\gamma = 0.1$**,** $\alpha_d = 0.01$**,** $Ec = 1.0$**,** $Nr = 0.1$**,** $N_B = 10.0$**,** $Ln = 100.0$ **and** $a = 0.3$**.**

Fig. 7 that except the heat transfer coefficient, all quantities shows a pronounced inclined for increasing values of particle-density increment. By increasing the particle density, the fluid near the surface will undergoes more resistance to flow and produces more frictional forces in boundary layer region, which ultimately enhance the skin friction coefficient(see Fig. 7(a)). As expected to see from Fig. 7(b) that the rate of heat transfer depicted by Q_w shows a significant decline by intensifying N_B. This may happen because of the presence of the nanoparticles in the base fluid results in a zig-zag motion of the particles which leads to collisions within the fluid as the particles interact hence increased heat production. Thus, an enhancement in values of particle-density increment number, N_B causes more collisions which generate more heat thus increasing the temperature and thus the rate of heat transfer is reduced at the surface of the vertical plate. The non-zero values of N_B drastically reduce the amplitude of the curve depicting the quantity, Q_w. Furthermore, it can be seen from Fig. 7(c), that the rate of mass transfer is very low for $N_B = 0.0$, and extensively promoted by increasing the values of N_B. Therefore, particle-density increment number has therefore great contribution in the flow region.

In order to illustrate the influence of mass concentration of dust particles parameter, D_ρ and amplitude of wavy surface a on streamlines and isotherms for water particulate suspension, Figs. (8) and (9) are plotted. These quantities help in visualizing and accessing the performance of the flow velocity and temperature fields of dusty fluid moving along the wavy surface. For comparison, suspension without particle cloud (pure water) is also presented in Fig. 8. As expected that by loading the dust particles, the velocity of dusty fluid reduces significantly as compared to clear fluid (pure water) as shown in Fig. 8(a).While

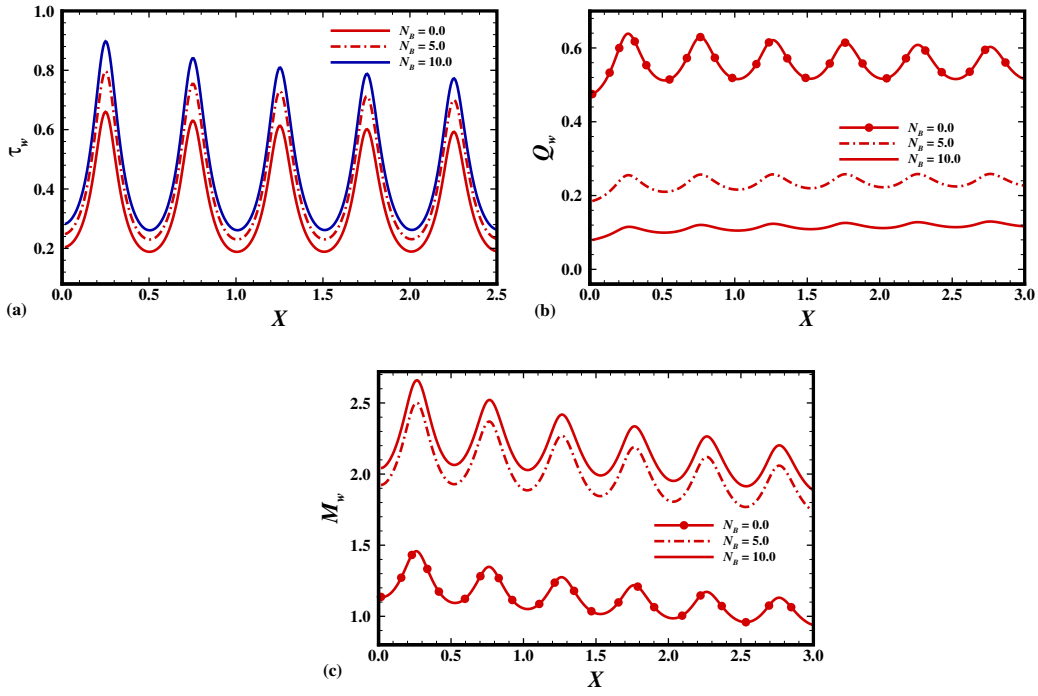

Fig. 7(a) τ_w, **(b)** Q_w **and (c)** M_w **for** $N_B = (0.0, 5.0, 10.0)$ **while** $D_\rho = 10.0$ **Pr** $= 7.0$, $\gamma = 0.1$, $\alpha_d = 0.01$, $Ec = 1.0$, $Nr = 0.1$, $N_A = 5.0$, $Ln = 100.0$ **and** $a = 0.3$**.**

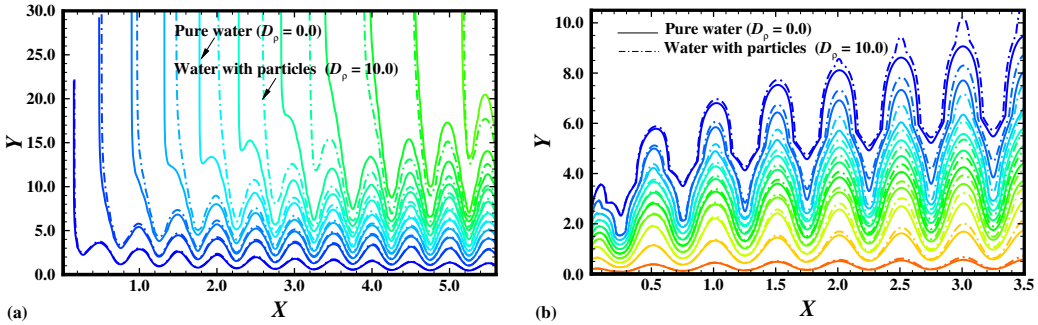

Fig. 8(a) Streamlines and (b) Isotherms for $D_\rho = (0.0, 10.0)$, **Pr** $= 7.0$, $\gamma = 0.1$, $\alpha_d = 0.01$, $Ec = 1.0$, $N_A = 5.0$, $N_B = 10.0$, $Ln = 100.0$, $a = 0.3$ **and** $Nr = 0.1$**.**

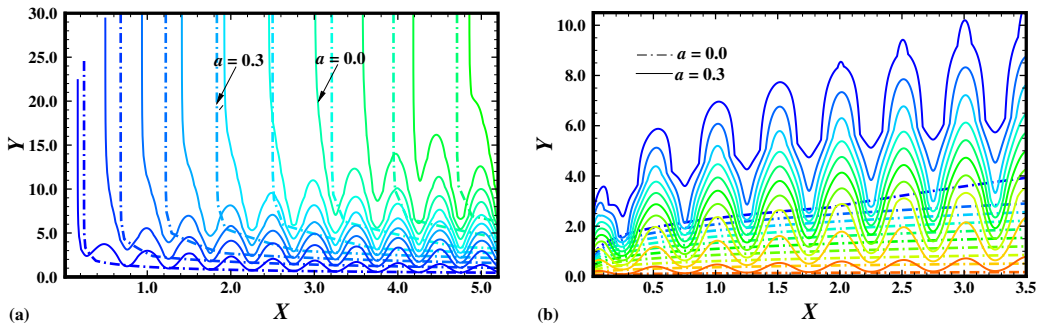

Fig. 9(a) Streamlines and (b) Isotherms for $a = (0.0, 0.3)$**, while** $D_\rho = 10.0$**,** $\mathbf{Pr} = 7.0$**,** $\gamma = 0.01$**,** $\alpha_d = 0.01$**,** $Ec = 1.0$**,** $N_A = 5.0$**,** $N_B = 10.0$**,** $Ln = 100.0$ **and** $Nr = 0.1$**.**

on the other hand, isotherms in Fig. 8(b) indicates that presence of dust particles have a notable influence on temperature distribution as isotherms get stronger for dusty water. When particles are loaded extensively, (i.e, $D_\rho = 10.0$), the inter-collisions of particles generate some thermal energy in base fluid, which ultimately increase the overall temperature into the boundary layer region. Besides, the amplitude of wavy surface extensively promote the fluid velocity as well as temperature distribution (see Fig. (9)). It is important to mention here that $a = 0.0$ represent the flat vertical surface. Particulary, the isotherms in Fig. 9(b), reveals the fact that the fluid accelerates more rapidly near the hot wavy surface and roughness of the plate is supportive driving force to increase the fluid temperature near the vicinity of wavy plate.

6 Conclusion

The present analysis aims to compute the numerical results of boundary layer flow of water-based dusty nanofluid along a vertical wavy surface. Primitive variable formulations are adopted, to transform the dimensionless boundary layer equations into convenient form and then the resulting nonlinear system of boundary layer equations are iteratively solved step-by-step by using implicit finite difference method along with tri-diagonal solver. Numerical results give a clear insight towards understanding response of the roughness of the surface. Effect of various emerging parameters are explored by expressing their relevance on skin friction coefficient, rate of heat transfer and rate of mass transfer. Velocity and temperature distributions are also plotted for carrier as well as particle phase. From this analysis, it is observed that modified diffusivity ratio parameter, N_A and particle-density increment number, N_B, has pronounced effect in reduction of heat transfer rate whereas reverse behavior is recorded in skin friction and rate of mass transfer under the influence of N_A and N_B. Moreover, the rate of heat transfer is extensively promoted by loading the mass concentration parameter, D_ρ.

References

[1] Choi, S., Enhancing thermal conductivity of fluids with nanoparticles, in: D. A. Siginer, H. P. Wang (Eds.), Development and Applications of Non-Newtonian Flows, ASME FED-231/MD, 66, 99-105, 1995.

[2] Das,S. K., Choi, S. U., Yu, W., Pradet, T., Nanofluids:Science and Technology, John Wiley & Sons, New Jersey, 2007.

[3] Buongiorno, J., Convective transport in nanofluids,*ASME J. Heat Transfer*, **128**, 240-250, 2006.

[4] Duangthongsuk, W., Wongwises, S., Effect of thermophysical properties models on the predicting of the convective heat transfer coefficient for low concentration nanofluid, *Int. Commun. Heat Mass Transfer*, **35**, 1320-1326, 2008.

[5] Wang, X. Q., Mujumdar, A., A review on nanofluidsPart I:Theoretical and numerical investigations, *Braz. J. Chem. Eng.*, **25**, 613-630, 2008.

[6] Kakaç, S., Pramuanjaroenkij, A., Review of convective heat transfer enhancement with nanofluids, *Int. J. Heat Mass Transfer*, **52**, 3187-3196, 2009.

[7] Lee, J. H., Lee, S. H., Choi, C. J., Jang, S. P., Choi, S. U. S., A review ofthermal conductivity data, mechanics and models for nanofluids, *Int. J. Micro-Nano Scale Transp.*, **1**, 269-322, 2010.

[8] Eagen, J., Rusconi, R., Piazza, R., Yip, S., The classical nature of thermal conduction in nanofluids, *ASME J. Heat Transfer*, **132**, 2010.

[9] Wong, K. F. V., Leon, O. D., Applications of nanofluids:current and future, *Adv. Mech. Eng.*, **11**, 519-659, 2010.

[10] Rudinger, G., Fundamentals of gas-particle flow, Elsevier Scientific Publishing Co., Amsterdam, 1980.

[11] Farbar, L., Morley, M. J., Heat transfer to flowing gas-solid mixtures in a circular tube, *Ind. Eng. Chem.*, **49**, 1957, 1143-1150.

[12] Saffman, P. G., On the stability of laminar flow of a dusty gas, *J. Fluid Mech.*, **13**, 1962, 120-128.

[13] Marble, F. E., Dynamics of a gas containing small solid particles, combustion and propulsion, 5th AGARD colloquium, Pergamon press, 1963.

[14] Singleton, R. E., Fluid mechanics of gas-solid particle flow in boundary layers, Ph.D. Thesis, California Institute of Technology, 1964.

[15] Michael, D. H., Miller, D. A., Plane parallel flow of a dusty gas, *Mathematica*, **13**, 1966, 97-109.

[16] Michael, D. H., The steady motion of a sphere in a dusty gas,*J. Fluid Mech.*, **31**, 1968, 175-192.

[17] Datta, N., Mishra, S. K., Boundary layer flow of a dusty fluid over a semi-infinite flat plate, *Acta Mech.*, **42**, 1982, 71-83.

[18] Agranat, V. M., Effect of pressure gradient of friction and heat transfer in a dusty boundary layer, *Fluid Dyn.*, **23**, 1988, 729-732.

[19] Roopa, G. S., Gireesha, B. J., Bagewadi, C. S., Numerical investigation of mixed convection boundary layer flow of a dusty fluid over an vertical surface with radiation, *Afr. Math.*, **24**, 2013, 487-502.

[20] Siddiqa, S., Hossain, M. A., Saha, S. C., Two-phase natural convection flow of a dusty fluid, *Int. J. Numer. Method*, **25**, 2015, 1542- 1556.

[21] Yao, L. S., Natural convection along a vertical wavy surface, *J. Heat Transfer*, **105**, 1983, 465-468.

[22] Moulic, S. G., Yao, L. S., Natural convection along a wavy surface with uniform heat flux, *J. Heat Transfer*, **111**, 1989, 1106-1108.

[23] Rees, D. A. S., Pop, I., Free convection induced by a vertical wavy surface with uniform heat flux in a porous medium, *J. Heat Transfer*, **117**, 1995, 545-550.

[24] Hossain, M. A., Pop, I., Magnetohydrodynamic boundary layer flow and heat transfer on a continuous moving wavy surface, *Arch. Mechanics*, **48**, 1996, 813-823.

[25] Hossain, M. A., Rees, D. A. S., Combined heat and mass transfer in natural convection flow from a vertical wavy surface, *Acta Mechanica*, **136**, 1999, 133-141.

[26] Siddiqa, S., Hossain, M. A., Saha, S. C., Natural convection flow with surface radiation along a vertical wavy surface, *Numerical Heat Transfer, Part A: Applications*, **64**, 2013, 400-415.

[27] Siddiqa, S., Hossain, M. A., Saha, S. C., The effect of thermal radiation on the natural convection boundary layer flow over a wavy horizontal surface, *Int. J. of Thermal Sciences*, **84**, 2104, 143-150.

[28] Pop, I., Natural convection of a darcian fluid about a wavy cone, *Int. Commun. Heat Mass transfer*, **21**, 1994, 891-899.

[29] Pop, I., Na, T. Y., Natural convection from a wavy cone, *Appl. Sci. Res.*, **54**, 1995, 125-136.

[30] Pop, I., Na, T. Y., Natural convection over a vertical wavy frustum of a cone, *J. Nonlinear Mechanics*, **34**, 1999, 925-934.

[31] Molla, M. M., Hossain, M. A., Gorla, R. S. R., Radiation effects on natural convection boundary layer flow over a vertical wavy frustum of a cone, *Proc. IMechE Part C: J. Mechanical Engineering Science*, **223**, 2009 1605-1614.

[32] Apazidis, N., Temperature distribution and heat transfer in a particle-fluid flow past a heated horizontal plate, *Int. J. Multiphase Flow*, **16**, 1990, 495-513.